Journal of Magnetics 7(2), 29-39 (2002)

A Study of Synthesis of NiCuZn-Ferrite Sintering in Low Temperature by Metal Nitrates and its Electromagnetic Property

Chul Won Kim* and Jae Gui Koh

Department of Physics, Soong Sil University, 1-1 Sangdo 5-Dong, Dongjak-Gu, Seoul 156-743, Korea

(Received 29 April 2002)

The initial NiCuZn synthetic ferrite were acquired from thermally decomposing the metal nitrates $Fe(NO_3)_39H_2O$, $Zn(NO_3)_26H_2O$, $Ni(NO_3)_26H_2O$, and $Cu(NO_3)_23H_2O$ at 150 °C for 24 hours, and then we calcined the synthetic powder at 500 °C, pulverized each of those for 3, 6, 9, 12, and 15 hours in a steel ball mill, sintered each at 700 °C to 1,000 °C for 1 hour, and thus studied their microstructures and electromagnetic properties. We could make the initial specimens chemically bonded in liquidity at a low-temperature 150 °C, by using the low melting points less than 200 °C of the metal nitrates instead of the mechanical ball-mill pulverization, then narrow a distance between the particles into a molecular one, and thus lower the reaction point of sintering by at least 200 °C to 300 °C. Their initial permeability was 50 to 400 and their maximum magnetic induction density and coercive force, 2,400 G and 0.3 Oe to 0.5 Oe respectively, which was similar to those of NiZnCu ferrite synthesized in the conventional process. In the graph of initial permeability by frequencies, a 180° rotation of the magnetic domain, which appears in a broad band of micro-wave before and after the resonance frequency, could be perceived.

Key words : Thermal Decomposition of Metal Nitrates, Low Temperature Sintered NiCuZn Ferrite

1. Introduction

By 1945 Snoek had laid the foundation of the physics and technology of practical ferrites, and a new industry came into being. Since that time the use of ferrites has become established in many branches of telecommunication and electronic engineering, and they now embrace a very wide diversity of compositions, properties and applications [1]. However, in recent days, the industry of electronic components, which is a basis of the electronics industry, is in continuous pursuit of miniaturization, light weight, high density, high performance, and multi functions as the SMT (Surface Mounting Technology) advances. In the latest developments in the electronics industry, the SMT is widely adopted instead of the insertion system of the leaded component [2-5]. Also, as miniaturization and thick film are preferred for the high performance of various electronic components, compared to the existing bulk types, a technology that not only has the same functions but can also improve the property is required. Especially, as the SMT advances, a ferrite component is also being converted into the shape of a multi-layer chip from the bulk, and in order to manufacture a chip ferrite component, although the ferrite as one of the magnetic materials is important, the development of an electric conduction material which can be co-fired with the ferrite and an appropriate printing technology are also important. Silver (Ag) is generally used as a internal conductor of the multi-layer ferrite chip, but as its melting point is 960.5 °C, developing a ferrite material which is sintering at a temperature less than 950 °C and establishing a sintering technology are necessary [5-7].

The methods which have been employed until recently for gaining a chemically homogeneous and fine powder are a coprecipitation reaction [8-12], a sol-gel reaction [12-15], a hydrothermal synthesis [16, 17], and a thermal decomposition of organic acid salt [18, 19] which has been recently applied in the synthesis of an high T_c oxide superconductors. In the other methods, except the organic-acid thermal decomposition, the metal alkoxide used as their raw material is expensive and takes a long time in its composition, and its powder has an unstable property that will hydrolyze by reacting to the moisture in the air. However, in the thermal decomposition of organic-acid salt, you can make the powder by heating organic salt in

*Corresponding author: Tel: +82-32-816-3094, e-mail: feone@nownuri.net

order to evaporate its solvents and then pyrolyzing it with the organic salt made after oxide or metal is melted in nitric acid and then, each metal ion is equally scattered [18-21]. This method has the merits that its raw material is not expensive; that its manufacture process is simple, and that you can acquire homogeneous and fine powder from it. Although the method used to acquire the powder in this syudy seems to be similar to that of the above thermal decomposition of organic-acd salt, in that the study used metal nitrates as starting materials, the thermal decomposition of organic-acid salt still remains intricate in that, in this method, the thermal decomposition and composition follow a complicated process to melt the starting material of metal oxide in nitric solution, to cause a reaction with citric acid, and to add ethylene glycol [21].

In this study, we used the metal nitrates $Fe(NO_3)_3 9H_2O$, $Zn(NO_3)_2 6H_2O$, $Ni(NO_3)_2 6H_2O$, and $Cu(NO_3)_2 3H_2O$ as starting materials, mixed the materials by fixed quantities by applying the weight percentages of the metal oxides which make up the ferrite, kept those in an electric oven at about 150 °C for 24 hours, and finally acquired the initial ferrite powder. We studied the microstructure and the crystal structures of the synthetic powder, took SEM and XRD for the powder specimen calcined by a 100 °C gap at 300 °C to 1100 °C, and especially investigated the microstructures and the electromagnetic properties of a ferrite sintering body resulting from the powder calcined especially at 500 °C.

2. The Method of Experiment

We filled a container with the metal nitrates which are $Fe(NO_3)_3 9H_2O$, $Zn(NO_3)_2 6H_2O$, $Ni(NO_3)_2 6H_2O$, $Cu(NO_3)_2 3H_2O$ as the starting materials which are gauged by fixed quantities according to the mol ratios of Fe, Zn, Ni, and Cu, based on the weight percentages of the basic metal oxides - Fe_2O_3(65.6 wt%), ZnO(17.3 wt%), NiO (6.7 wt%), and CuO(10.4 wt%), put them in an electric oven at about 150 °C, thermally decomposed them for 24 hours, and finally acquired a NiCuZn synthetic ferrite powder which has a homogeneous composition. Simultaneously, for TG analysis, we studied the thermal decomposition process of the metal nitrates, by conducting a thermal analysis of the metal nitrate mixture at room temperature to 1,000 °C with an increasing rate of temperature of 2.5 °C/min.

We calcined the synthetic powder resulted from the thermal decomposition at 300 °C to 1,100 °C with a 100 °C interval for one hour each, pulverized the calcined sample with a pestle, measured the size of the granule resulted from the pulverization with a particle analyzer (Malvern Mastersizer: Ver. 2.19), and observed the shape of the powder with a SEM. We examined the quantity of the produced spinel structure, by analyzing the shape of the powder synthesized by the thermal decomposition and that of the powder calcined at each temperature with an X-Ray Diffractometer (XRD).

For the sample calcined at 500 °C for 1 hour, we splitted it by a fixed quantity of 600 g and conducted a wet ball milling for 3, 6, 9, 12, and 15 hours respectively. After the milling operation, we acquired the powder of each specimen after drying it at about 150 °C, analyzed the granularity of a part of the powder for examining the difference of its granularity which may have been appeared after the wet ball milling pulverization, granulized the rest of the powder and passed the granules through 40 meshes, molded the passed granule powder to be 9.0 g to 9.2 g in weight and 11.3 mm to 11.4 mm in height with a toroidal type mold of 21.2 mm (outer diameter) × 11.4 mm (inner diameter), and finally acquired the specimens sintered at 700 °C, 800 °C, 900 °C, and 1,000 °C each for 1 hour. For the sintered bodies, we studied properties of initial permeability, Q-value, and impedance by their frequencies (1 MHz to 1 GHz) according to the condition of sintering temperatures and milling times, and measured the maximum magnetic induction density (B_m), the residual magnetic induction density (B_r), and the coercive force (H_c) of each sample with a B-H curve tracer. We observed the cross sections of the sample fragments through the SEM photographs and examined their relations with sintering temperatures.

3. Results and Discussion

In Fig. 1, we showed a SEM photograph of fine structures and a result of granularity distribution of the particles resulting after pulverizing with a pestle the ferrite powder acquired from the thermal decomposition of the metal nitrates. We can see in the Fig. 1(a) picture that the particles of the powder are fine because their size do not exceed 1 μm, that they are round-shaped, and that their particles are united to make up masses. We can see in the granularity distribution of the Fig. 1(b) that there are several peaks and many particles larger than 10 μm. As shown in the figures, we think that the large particles are the result of the union of those fine particles that were not perfectly pulverized. Accordingly, if only the particles whose granularities are small are considered, those below 0.5 μm can be judged as fine.

In Fig. 2, we showed the diffraction pattern resulting from examining the homogeneity of the chemical com-

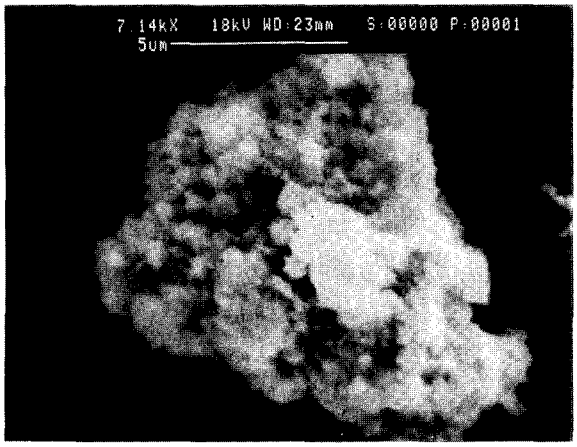

(a)

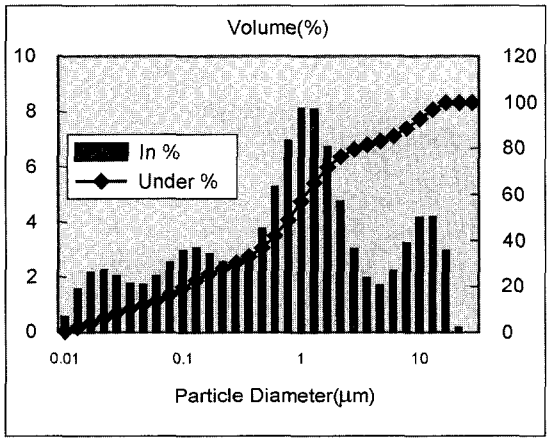

(b)

Fig. 1. (a) SEM photographs and (b) particle size distribution of the powder obtained after pulverizing with a pestle the ferrite powder acquired from the thermal decomposition of the metal nitrate mixture.

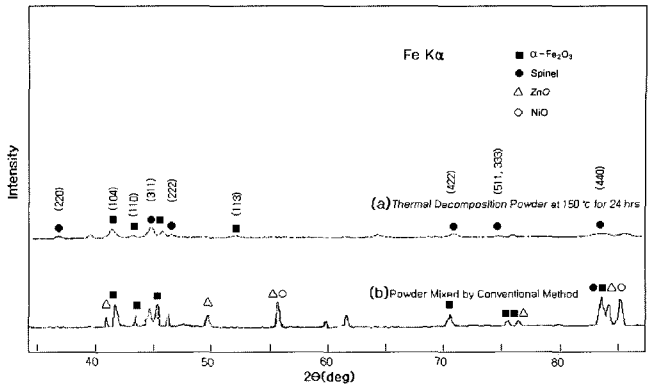

Fig. 2. X-ray diffraction patterns of (a) the thermal decomposition powder of metal nitrates and (b) the powder mixed by the conventional method.

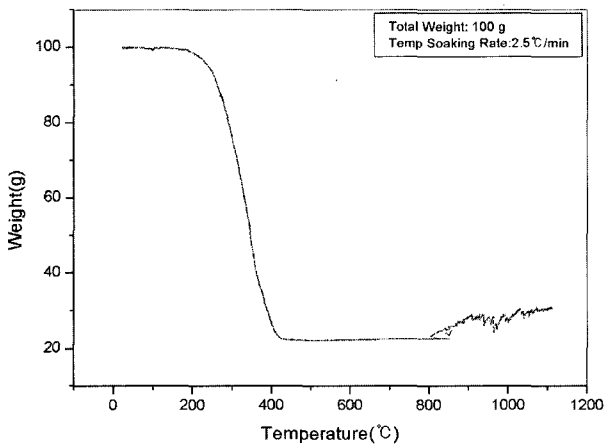

Fig. 3. TG graph on NiCuZn ferrite powder synthesized from metal nitrate mixture.

position of the ferrite powder acquired by the thermal decomposition of the metal nitrates with X-ray diffraction (XRD). For a comparison, the diffraction pattern [22] of the powder for which the metal oxides are mixed in the conventional process is also shown. Although the diffraction of each oxide clearly appeared in the diffraction pattern of the mixed powder in Fig. 2(b), it was reduced in the diffraction pattern of the powder synthesizeded by the thermal decomposition of the metal nitrates in Fig. 2(a). Only the main peaks which included (104) and (110) of Hematite (α-Fe_2O_3) [23], (101) of ZnO, (200) of NiO, and (111) of CuO weakly appeared, and the new spinel phase 2θ appeared near 37°, 45°, 47°, 76°, and 84°. The peaks of NiCuZn synthetic ferrite powder in Fig. 2(a) were shown in (220), (311), (222), (511, 333), and (440) which appears in typical spinel structure (cf. Fig. 4). The amount of the spinel phase was calculated to be about 50% using the internal standard method [24] that represents the ratio of the strength of the spinel (311) against that of the hematite (104). That the spinel phase was formed really proves that the method of the thermal decomposition of the metal nitrates homogenizes the composition of ferrite and shows that the calcinations can be conducted at a lower temperature and that the sintering also can be conducted at a temperature lowered by a large range.

We showed the result of the TG analysis in Fig. 3 in order to examine the timing for the powder made by the thermal decomposition of the metal nitrates to change perfectly into ferrite. In the figure, the reduction of weight, starting from 200 °C, is completely terminated by 400 °C. This shows that the changing into ferrite is already complete near the point of 400 °C. It shows that we can lower the conventional calcining point of around 850 °C and sintering point of above 1,000 °C by 200 °C to 400 °C.

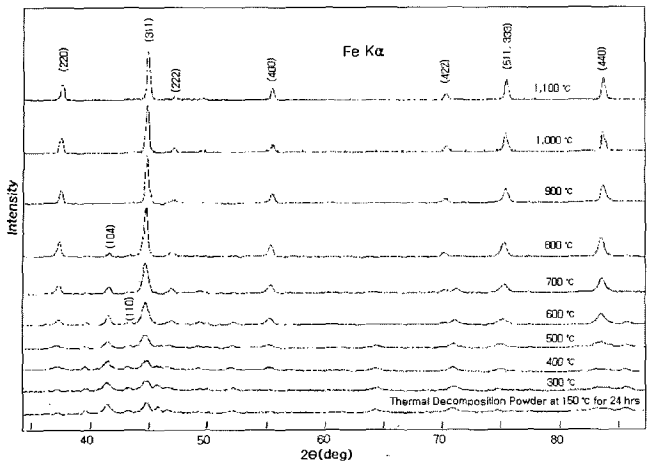

Fig. 4. XRD patterns of the powder by thermal decomposition of metal nitrates and the specimens calcined at 300 °C to 1,100 °C for 1 hr.

In Fig. 4, we showed the spinel quantity resulting from calcining the powder acquired by the thermal decomposition of the metal nitrates in the air at 300 °C to 1,100 °C by a 100 °C gap for 1 hour each, examined by XRD. The peaks of the oxides such as Fe_2O_3, ZnO, and NiO appear weakly in low calcining temperatures, only the peak [23] of (104) of Fe_2O_3 appears as the calcining temperature increases. The spinel quantities when calcined at more than 800 °C were above 98%. We showed a corresponding SEM picture in Fig. 5. It shows that the particle is growing as the calcining temperature increases. The granularity distribution of the calcined powder is also showed in Fig. 6. A regular tendency in the particle distribution according to the increase of the calcining temperature was not discovered here. Fig. 5 shows that the particle size becomes larger as the calcining temperature increases,

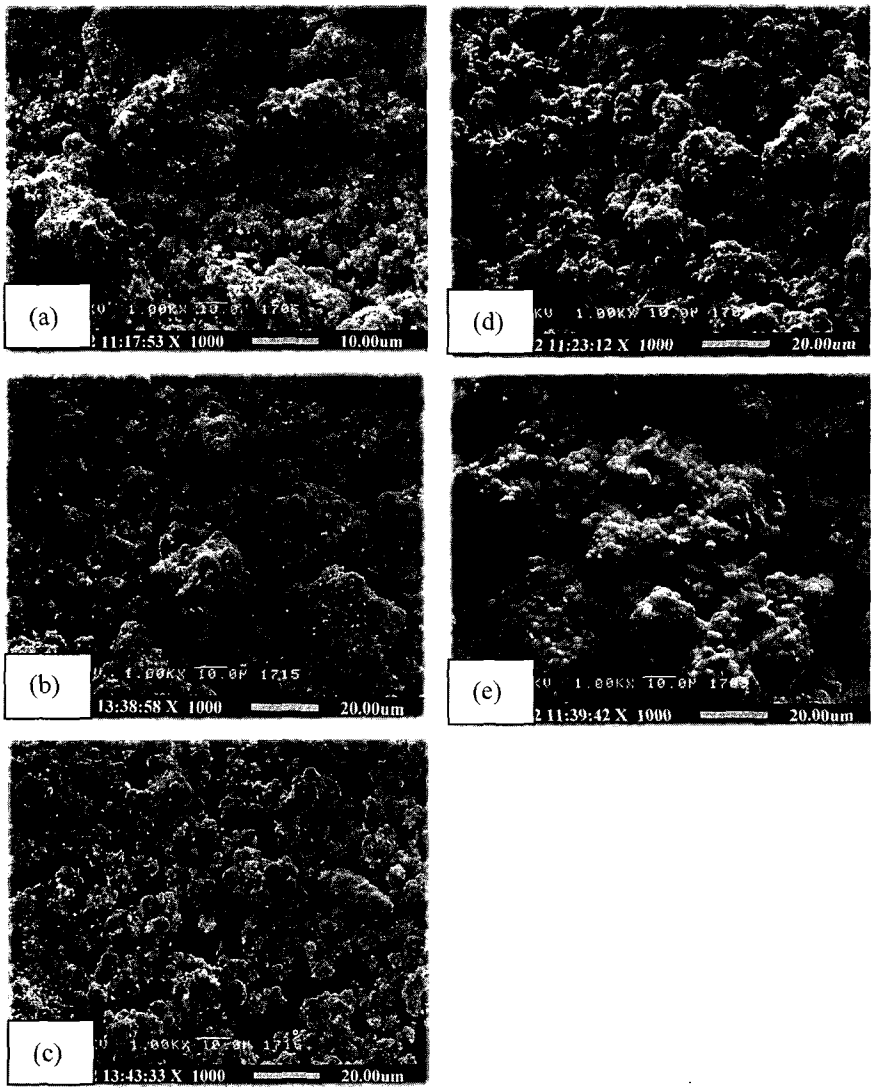

Fig. 5. SEM photographs of the powder specimens calcined at (a) 300 °C, (b) 500 °C, (c) 700 °C, (d) 900 °C, and (e) 1,100 °C respectively for 1 hr after thermal decomposition.

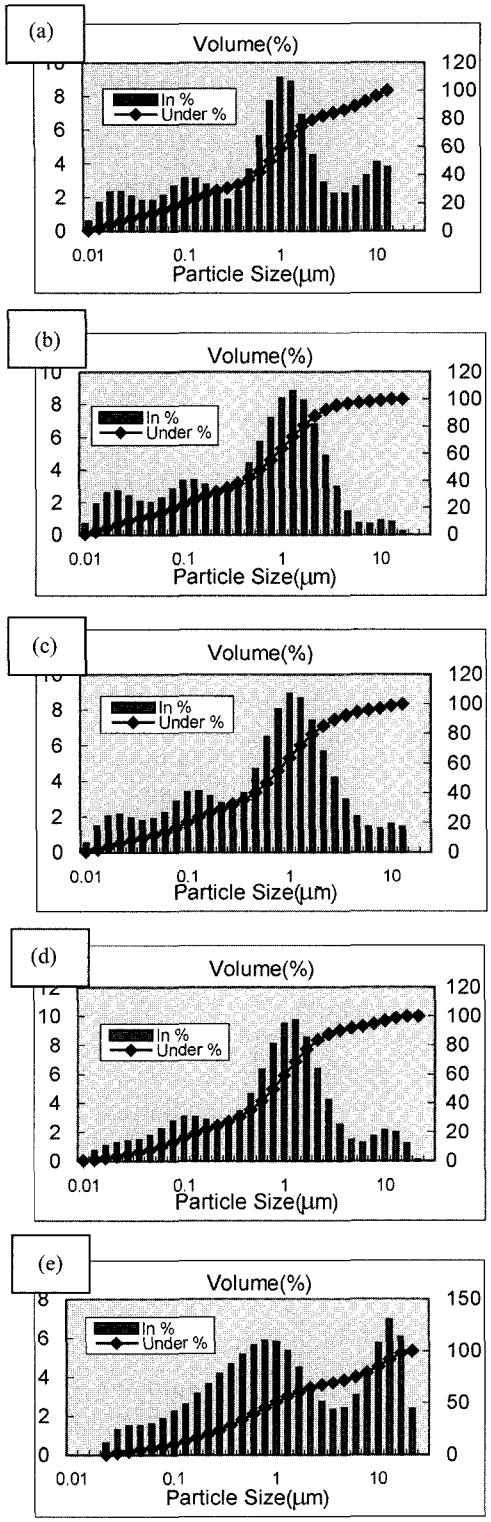

Fig. 6. Particle size distribution of the powder specimens calcined at (a) 300 °C, (b) 500 °C, (c) 700 °C, (d) 900 °C, and (e) 1,100 °C each for 1 hr after thermal decomposition.

demonstrating the sintering phenomenon in which the particle size grows by calcining. As the calcined particles

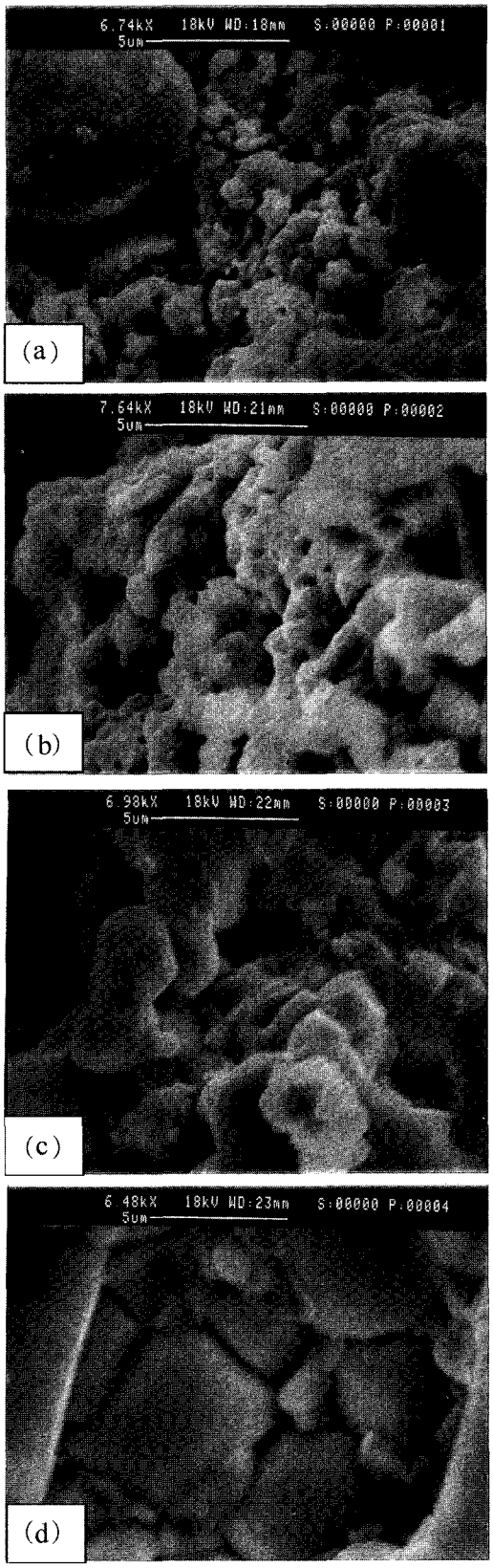

Fig. 7. SEM photographs of specimens sintered at (a) 700 °C, (b) 800 °C, (c) 900 °C, and (d) 1,000 °C each for 1 hr after being calcined at 500 °C for 1 hr.

are measured after being pulverized by a pestle, it shows that the distribution of granularity largely depends on the degree of the pulverization by the pestle. Several peaks appear in the figure and it is assumed that the large particles of more than 10 μm are those into which fine grains are condensed, as shown in Fig. 5. Accordingly, it is judged that a real average granularity will be below 0.5 μm.

Fig. 7 shows the result of a SEM examination of the cross-sections of the sample fractions which were sintered at 700 °C to 1,000 °C for 1 hour after being calcined at 500 °C for 1 hour and then wet ball milled for 3, 6, 9, 12, and 15 hours respectively. Pores decreased as the sintering temperature increased. The grains of ferrite grew as the sintering temperature increased. The pores of the specimens sintered at 800 °C mostly existed near the boundary at which the particles met each other, their average size was about 2 μm, and the distribution of their particles was comparatively inhomogeneous. Otherwise, for the specimens sintered at 1,000 °C, compared to those sintered at 800 °C, the number of pores decreased, their sizes became a little larger, and they were evenly dis-

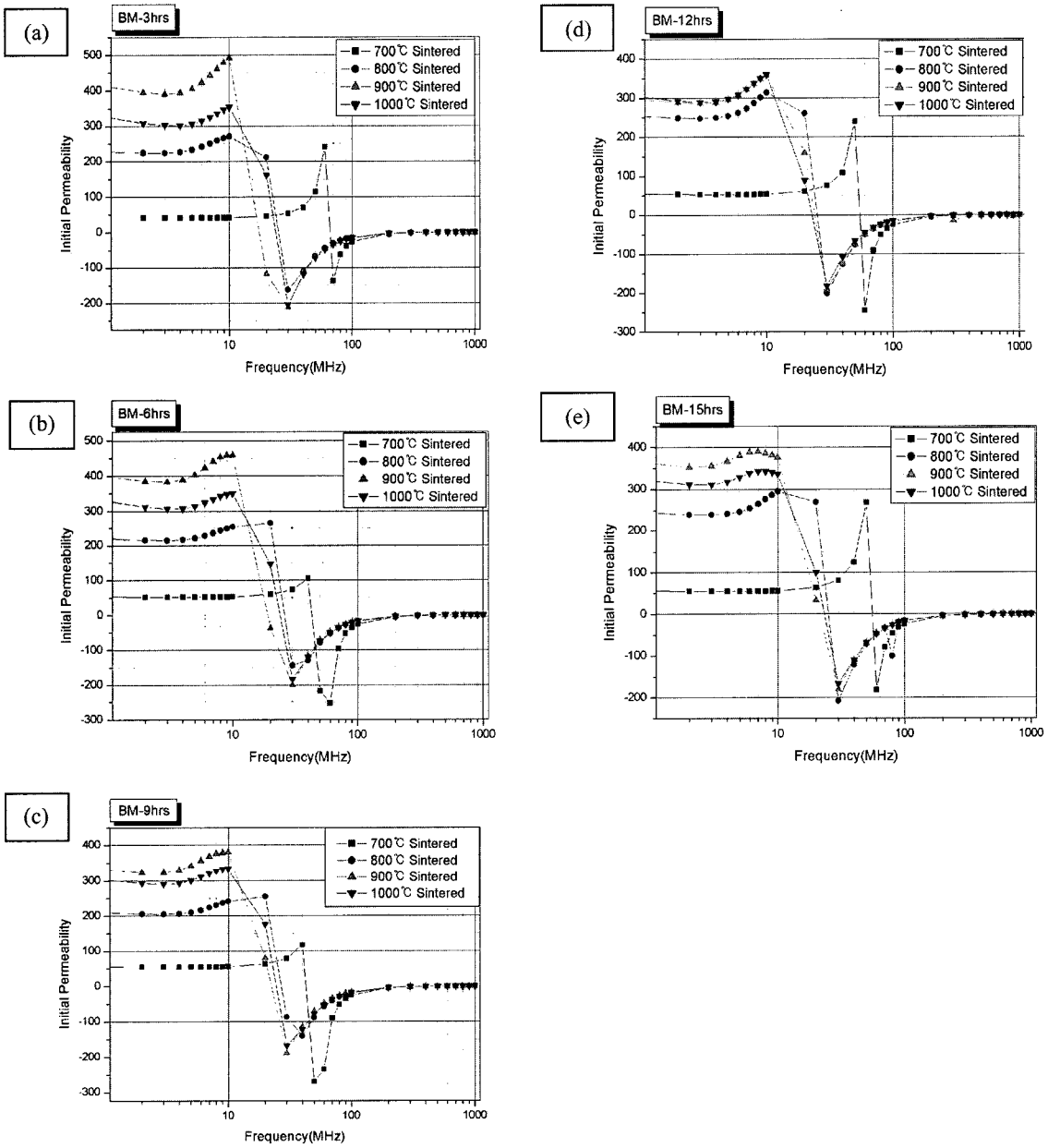

Fig. 8. Initial permeability vs. frequency for sintering temperatures of 700 °C, 800 °C, 900 °C, and 1,000 °C respectively according to milling times of (a) 3 hrs, (b) 6 hrs, (c) 9 hrs, (d) 12 hrs, and (e) 15 hrs each.

tributed at the boundary and at the inside of the boundary. The average size of the particles became considerably largeer to above 5 μm, abnormal growth of the particles was frequently observed. Those fine structures were acquired at a sintering temperature lower by about 200 °C to 300 °C than that of when the mechanically mixed powder was used. Although the electromagnetic property of ferrite is at its best at an appropriate sintering temperature, a high sintering temperature is beneficial for the densification of the sintering body, but disadvantageous as it causes the continuous growth of the particles. In order to prevent this, we need to add an agent restraining the growth of the particles or to lower the sintering temperature. By doing so, we can make the frequency property of ferrite favorable and acquire a ferrite which has a more stable property as a low-temperature sintering body.

Fig. 8 shows initial permeability *vs.* frequency for sintering temperatures of 700 °C, 800 °C, 900 °C, and 1,000 °C respectively according to milling times of (a) 3 hrs, (b) 6 hrs, (c) 9 hrs, (d) 12 hrs, and (e) 15 hrs each. The initial permeabilities (at 1 MHz) of the specimens sintered at 700 °C to 1000 °C appeared to be 50, 210~260, 300~410, and 300~350 at each sintering temperature. As

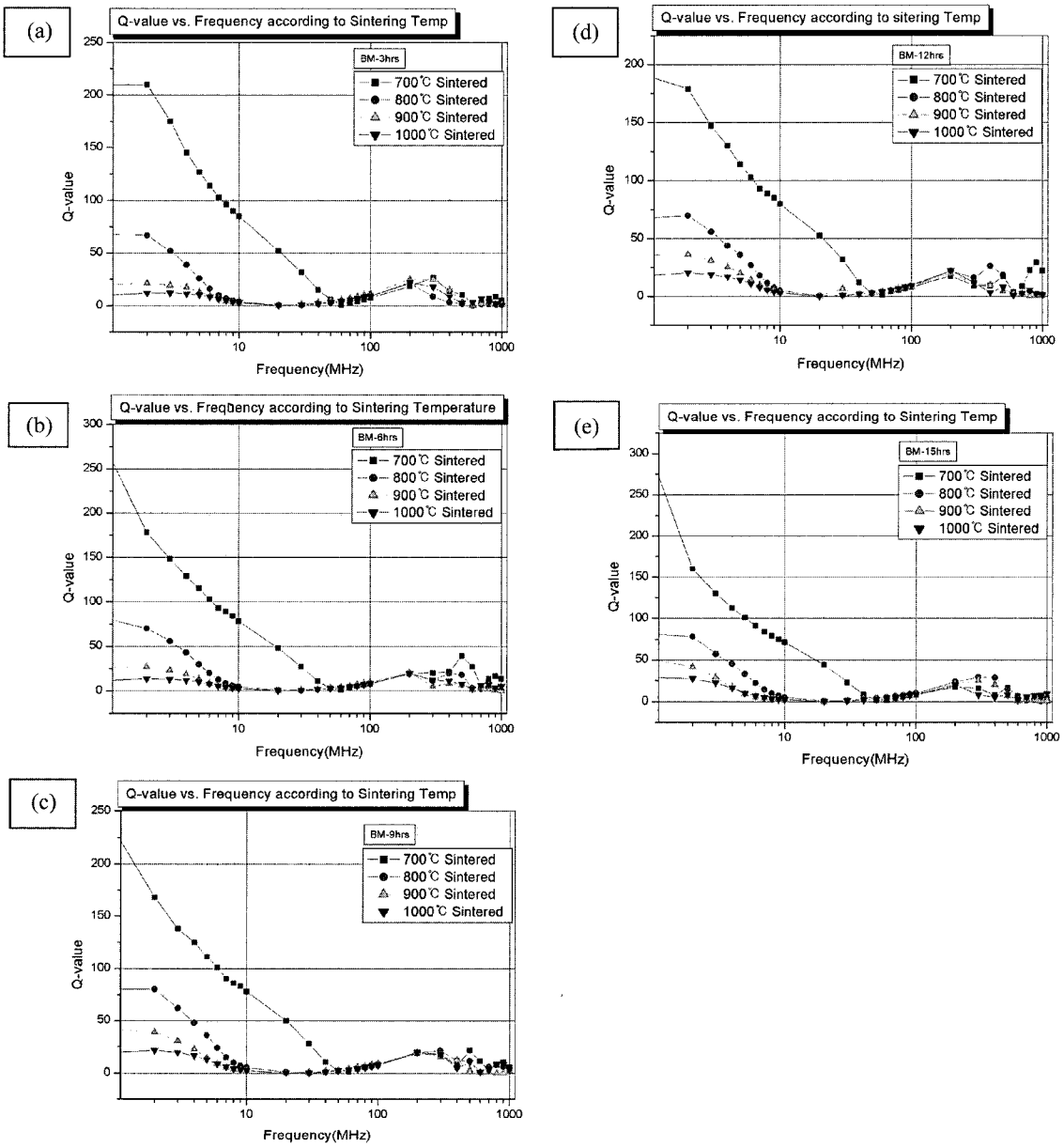

Fig. 9. Q-value vs. frequency for sintering temperatures of 700 °C, 800 °C, 900 °C, and 1,000 °C each for 1 hr according to milling times of (a) 3 hrs, (b) 6 hrs, (c) 9 hrs, (d) 12 hrs, and (e) 15 hrs respectively after calcining at 500 °C for 1 hr.

the sintering temperature was going up, the milling effect could be clearly seen, and the maximum value of permeability 410 appeared in the specimens sintered at 900 °C which were milled for 3 to 6 hours. However, the initial permeability of the specimens sintered at 1000 °C decreases, which is supposedly caused by that, although the sizes of the particles increase a great deal, the permeability decreases due to a pinning phenomenon which occurs when the magnetic wall moves, as the small pores on the inside of the crystal particle decrease but the developing pores become larger when the crystal particle grows up [25]. It represents that, although we cannot verify the movement of the resonance frequency by milling times, the change of initial permeability by the milling effect, that is, the sintering effects on the growth of particles. As the sintering temperature increased, the initial permeability increased but the resonance frequency moving towards a low frequency. This can be explained by equation (1) [26] below.

$$\omega\mu = 2\upsilon I_s/(3\ \mu_0) \tag{1}$$

In the equation, each letter means the following - ω:

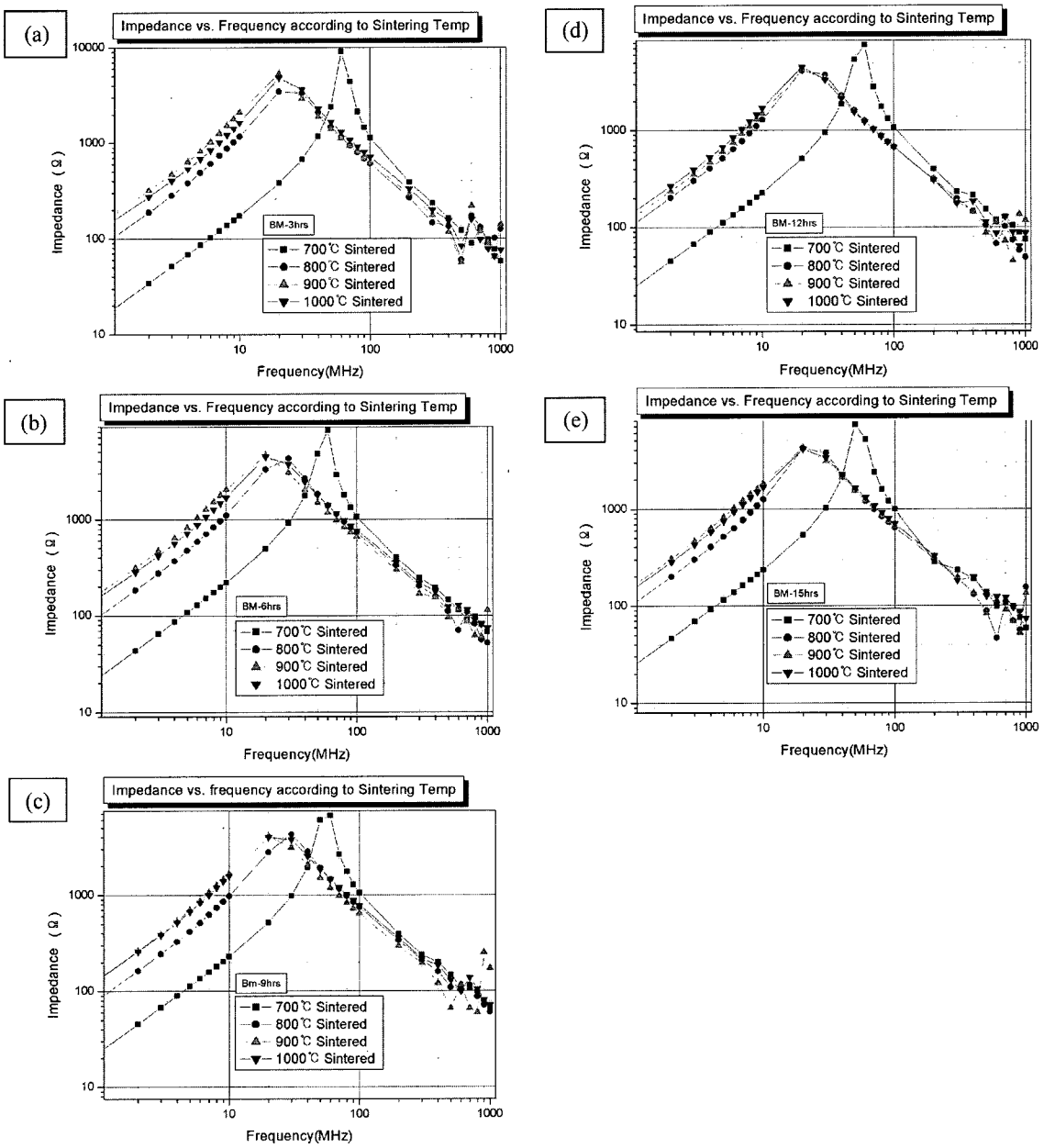

Fig. 10. Impedance vs. frequency for sintering temperatures of 700 °C, 800 °C, 900 °C, and 1,000 °C according to milling (a) 3 hrs, (b) 6 hrs, (c) 9 hrs, (d) 12 hrs, and (e) 15 hrs respectively after calcining at 500 °C for 1 hr.

resonance frequency, μ: relative magnetic permeability, υ: an invariable of magnetic rotation, I_s: saturated magnetization, and μ_0: permeability in a vacuum. When we apply $\omega = 2\ \pi f$, (f: frequency), a line whose permeability rapidly decreases arrives at the limit-line of Snoek [26], and the resonance frequency decreases when the initial permeability increases due to an inversely proportionate relationship between the resonance frequency and the initial permeability. The result of the experiment meets the limit-line of Snoek and corresponds with the presupposition of the numeral formula. Fig. 8 shows that the direction of the magnetic domain rotates by 180°. Supposedly, it is caused by the phenomenon of Fraday rotation [27] due to the strong magnetic resonance usually appearing in the micro-frequency broad bands of 300 MHz to 3 GHz. It is supposed that the magnetization increases, but that the resonance frequency decreases as the Q-value decreases according to the increase of frequency, as shown in Fig. 9. The lowered Q-value caused by the change of frequency can be explained by the

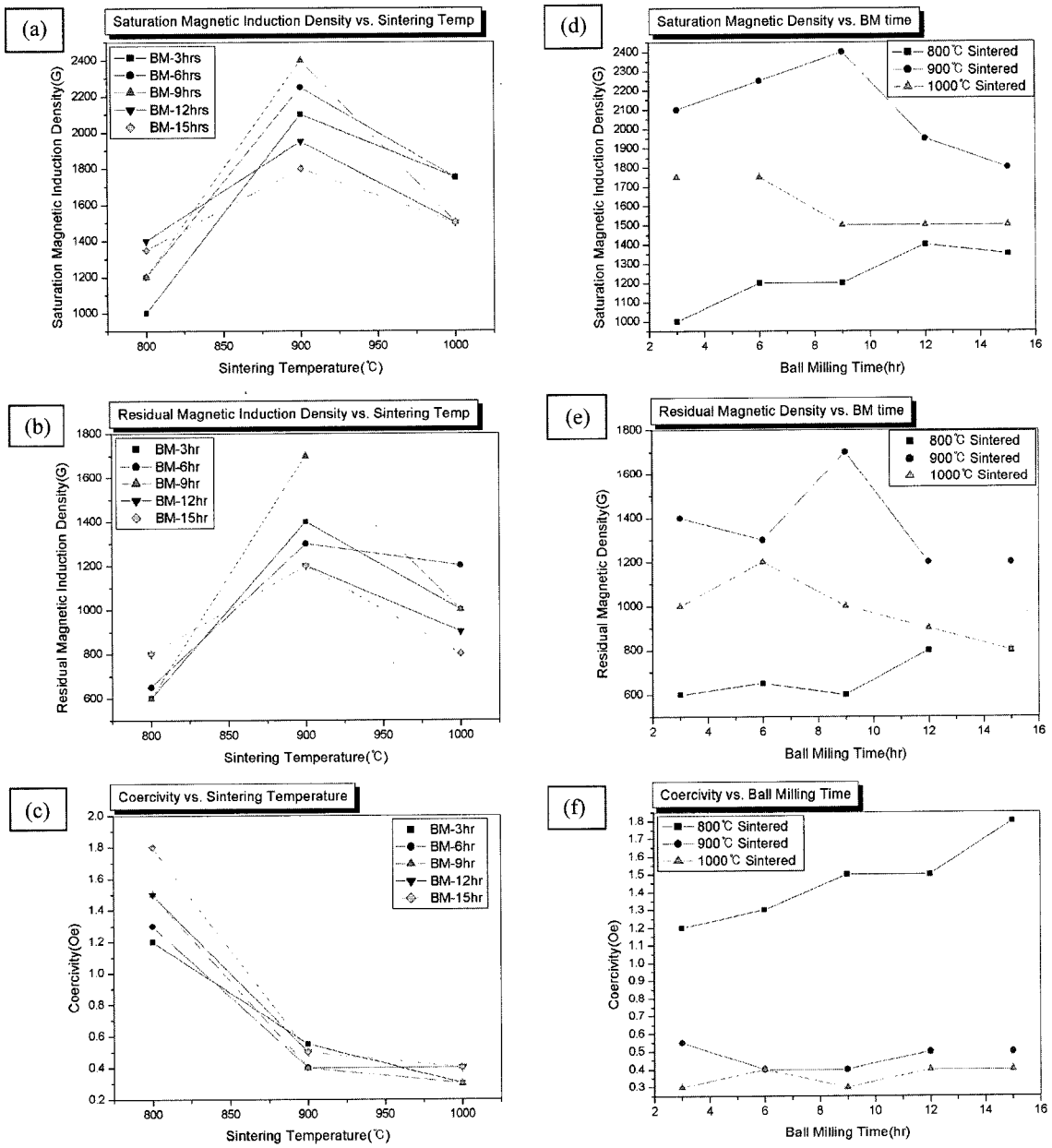

Fig. 11. (a) saturation magnetic induction density, (b) residual magnetic induction density, and (c) coercivity for sintering tempratures according to milling times of 3 hrs, 6 hrs, 9 hrs, 12 hrs, and 15 hrs; and (d) saturation magnetic induction density, (e) residual magnetic induction density, and (f) coercivity for milling times according to sintering temperatures of 700 °C, 800 °C, 900 °C and 1,000 °C after calcining at 500 °C for 1 hr.

following equation (2) [28] which shows the relation between Q and the initial permeability.

$$\frac{\tan\delta}{\mu_i} = \frac{1}{\mu_i Q} \quad (2)$$

Fig. 10 shows that the impedance varies with frequency. Since the impedance is A.C. resistance in which the initial permeability and the resistance are mixed, it has a curve similar to that of the initial permeability; however, the fact that the curve does not rise but declines at more than the resonance frequency is supposedly because the initial permeability becomes larger than 1. The resonance frequency of specimens ranged from 10 MHz to 60 MHz.

Fig. 11 shows the relations among the maximum magnetic induction density (B_m), the residual magnetic induction density (B_r), and the coercive force (H_c). Generally, as the sintering temperature increases, the maximum magnetic induction density and the residual magnetic induction density increase, but the coercive force decreases. Also in this experiment, as the sintering temperature increases, the maximum magnetic induction density and the residual magnetic induction density increase. This is due to the fact that the magnetic induction density is closely related to the densification of the sintering body, that is, that the reduction of the pores which formulate the demagnetizing field in the inside of the crystal particle increases the magnetic induction density [29]. It is shown that the densification and maximum magnetic indensity appeared at the sintering point of 900 °C and at the milling point of 9 hours. At the temperature above 900 °C, the over-expanded pore was supposedly a reason causing the magnetic induction density to decrease. As shown in the picture, the coercive force decreases in proportion to the sintering temperatures and shows some differences caused by the milling conditions. The highest points of the maximum magnetic induction density and the residual magnetic induction density appeared 2400 G and 1700 G respectively in the specimens sintered at 900 °C with a 9 hr milling time. The minimum value of the coercive force was shown at 1,000 °C with a 9 hr millimg time. It is judged that, in the study, the milling effect after calcining appearing only a little is because the granularity of the initial NiCuZn synthetic ferrite specimen synthesized by the thermal decomposition of the metal nitrates was less than 0.5 um.

4. Conclusion

For the sample material, we used the low temperature sintering NiCuZn Ferrite powder synthesized by the thermal decomposition of the metal nitrates, and analyzed the distribution of the granularities, the microstructures, and the XRD patterns of the powders acquired from calcining the NiCuZn synthetic ferrite powder at 300 °C to 1,100 °C each. Also, through a TG analysis which shows the decomposition point of the metal nitrate mixture, especially through the result of analyzing the microstructures and the electromagnetic property of the specimens resulting from sintering at 700 °C, 800 °C, 900 °C, and 1,000 °C each, of the specimens acquired from differentiating the milling times at 3, 6, 9, 12, and 15 hours for the powder calcined at 500 °C for 1 hour, we reached the following conclusions.

1. We did not discover that the distribution of the granularity moves towards the fine particles at the range of 0.01 um to 50 um as the milling time increases. It is judged that milling effect did not appear since the thermal decomposiontion of metal nittrates had already made infinitesimal particles. Adjudging from that the masses into which the granules less than 1um are united are shown in the SEM pictures, the real sizes of the particles are less than 0.5 um.

2. A spinel phase of the sample acquired from conducting the thermal decomposition at 150 °C for 24 hours at first was already being formed. And the result of TG graph also shows that the decomposition started at 200 °C and was already completed at 400 °C, with a ferrite phase completed.

3. The SEM results of the initial thermally-decomposed samples and the powder samples acquired from heating at 300 °C to 1,100 °C show that, in the samples clacined at high temperature, the particles are changed into an agglomerates by a solid state reaction, although we cannot clearly distinguish it as the changes of the fine granules are too minute. In the XRD pattern, a spinel phase appeared from the initial sample of thermal decomposition and the spinel peaks showed their maximum strengths at more than 700 °C.

4. The SEM result of the sintering body shows that the grain grew as the sintering temperature increased. However, the excessive growth of the grain played a role in lowering the initial permeability and the maximum magnetic induction density.

5. It can be assumed that an optimum sintering temperature for the initial permeability, the maximum magnetic induction density, and the coercive force can be fixed in the range of 800 °C to 900 °C. The results of the TG graph and XRD pattern show that the calcining temperature can be lowered to around 400 °C.

6. The band of the resonance frequency moved to a high frequency band (~100 MHz) as the sintering temperature beccame lower. The properties of the initial perme-

ability, impedance, maximum magnetic induction density (B_m), and residual magnetic induction density (B_r) increased as the sintering temperature increased, but they decreased at the maximum sintering temperature 1,000 °C, which was supposedly caused by the appearance of an abnormal grain and large pores inside the grain boundary.

To study the composition change of metal nitrates by thermal decomposition and variable additive tests will be the subject of future study in seeking a lower sintering point.

References

[1] E. C. Snelling, *Soft Ferrites/properties and applications 2nd ed.*, Butterworths, London (1988), pp.1.

[2] H. Momoi, A. Nakano, and T. Nomura, Ferrites: Proc. of ICF**6**, 1202 (1992).

[3] Masayuki Fujimoto, J. Am. Ceram. Soc. **77**(11), 2873 (1994).

[4] A. Nakano, T. Aoki, H. Momoi, T. Suzuki, and T. Nomura, Ferrites: Proc. of ICF**8**, 1117 (2000).

[5] N. Taguchi, T. Yamaguchi, Y. Okino, and H. Kishi, Ferrites: Proc. of ICF**8**, 1122 (2000).

[6] J. H. Nam, H. H. Jung, J. Y. Shin, and J. H. Oh, IEEE Trans Magn. **31**(6), 3985 (1995).

[7] Lu Mingyue, Ferrites: Proc. of ICF**8**, 1151 (2000).

[8] J. H. Lee, J. G. Koh, J. of Kor. Mag. Soc. **11**(5), 218 (2001).

[9] D. W. Johnson, Jr., Am. Ceram. Bull. **60**(2), 221-224 (1987).

[10] Suzilene R. Janasi, Daniel Rodrigurs, Fernando J. G. Landgraf, and Mafilia Emura, IEEE Tran. Magnn. **36**(5), 3327 (2000).

[11] R. E. Park, N. K. Kang, K. H. Park, and J. H. Oh, J. of Kor. Inst. of Metals **28**(11), 983 (1990).

[12] W. C. Kim, S. J. Kim, Y. R. Uhm, and C. S. Kim, IEEE Trans. Magn. **37**(4), 2362 (2001).

[13] Y. J. Oh, H. S. Choi, and J. Y. Choi, J. of Kor. Cer. Soc. **37**(5), 55 (2000).

[14] S. Y. Ann, G. J. Yang, and Y. G. Ryu, J. of Kor. Mag. Soc. **11**(4), 168 (2001).

[15] W. C. Kim, Y. S. Yi, and C. S. Kim, J. of Magnetics **5**(4), 111 (2000).

[16] K. H. Yi, B. H. Yi, and S. G. Kim, J. of Kor. Cer. Soc. **24**(1), 18 (1987).

[17] J. S. Kim, J. R. Ann, and H. J. Ryu, Kor. J. of Materials Research **10**(3), 224 (2000).

[18] T. Asaka, Y. Okazawa, and K. Tachikawa, J. of Japan Inst. of Metals, **56**(6), 715 (1992).

[19] T. Asaka, Y. Shiomi, and K. Tachikawa, J. of Japan Inst. of Metals **56**(6), 722 (1992).

[20] J. W. Jung, and W. J. Yi, J. of Kor, Powder Metallurgy Inst. **2**(1), 29 (1995).

[21] J. W. Jung, and W. J. Yi, Kor. J. of Materials Research **5**(5), 513 (1995).

[22] J. W. Jung, and W. J. Yi, J. of Kor, Powder Metallurgy Inst. **2**(1), 31 (1995).

[23] Kato, M. J. Kim, and I. H. Seo, Analysis of X-ray diffraction, Bando Pubsishing Co. (1993), pp.211.

[24] B. D. Cullity, *Elements of X-Ray Diffraction 2nd ed.*, Addison-Wisley Publishing Co., Inc. (1978), pp.360-363.

[25] H. W. Cho, S. B. Jin, H. W. Moon, and Y. J. Shin, J. of Kor. Inst. of Electrical and Electronic Materials Engineers, **8**(6), 748 (1995).

[26] Soshin Chikazumi, *Physics of Ferromagnetism 2nd ed.*, Clarendon Press, Oxford (1997), pp.556-562.

[27] Alex Goldman, *Handbook of Modern Ferromagnetic Materials*, Kluwer Academic Publishers, Boston/Dordrecht/London (1999), pp.71-72.

[28] J. G. Koh, and J. M. Song, Basics and Applications of Magnitic Physics, Soongsil Uni. Press, Seoul (2001), pp.176.

[29] J. G. Koh, and J. M. Song, Basics and Applications of Magnitic Physics, Soongsil Uni. Press, Seoul (2001), pp.186.